Received: 26 October 2020 | Revised: 1 February 2021 | Accepted: 3 February 2021

DOI: 10.1002/jcb.29909

RESEARCH ARTICLE

Journal of Cellular Biochemistry WILEY

Tetracycline as an inhibitor to the SARS-CoV-2

Tom Y. Zhao | **Neelesh A. Patankar**

Department of Mechanical Engineering, Northwestern University, Evanston, Illinois, USA

Correspondence
Tom Y. Zhao and Neelesh A. Patankar, Department of Mechanical Engineering, Northwestern University, Evanston, IL 60208, USA.
Email: tomzhao@u.northwestern.edu (T.Y.Z.) and n-patankar@northwestern.edu (N.A.P.)

Abstract

The coronavirus severe acute respiratory syndrome coronavirus 2 (SARS-CoV-2) remains an extant threat against public health on a global scale. Cell infection begins when the spike protein of SARS-CoV-2 binds with the human cell receptor, angiotensin-converting enzyme 2 (ACE2). Here, we address the role of tetracycline as an inhibitor for the receptor-binding domain (RBD) of the spike protein. Targeted molecular investigation show that tetracycline binds more favorably to the RBD (−9.40 kcal/mol) compared to doxycycline (−8.08 kcal/mol), chloroquine (−6.31 kcal/mol), or gentamicin (−4.83 kcal/mol) while inhibiting attachment to ACE2 to a greater degree (binding efficiency of 2.98 kcal/(mol nm^2) for tetracycline–RBD, 5.16 kcal/(mol nm^2) for doxycycline–RBD, 5.59 kcal/(mol nm^2) for chloroquine–RBD, and 7.02 kcal/(mol nm^2) for gentamicin–RBD. Stronger inhibition by tetracycline is verified with nonequilibrium PMF calculations, for which the tetracycline–RBD complex exhibits the lowest free energy profile along the dissociation pathway from ACE2. Tetracycline binds to tyrosine and glycine residues on the viral contact interface that are known to modulate molecular recognition and bonding affinity. These RBD residues also engage in significant hydrogen bonding with the human receptor ACE2. The ability to preclude cell infection complements the anti-inflammatory and cytokine suppressing capability of tetracycline; this may reduce the duration of ICU stays and mechanical ventilation induced by the coronavirus SARS-CoV-2.

KEYWORDS

Coronavirus, COVID-19, SARS-CoV-2, tetracycline

1 | INTRODUCTION

The extreme urgency for therapeutics against the severe acute respiratory syndrome coronavirus 2 (SARS-CoV-2) drives the review of existing drugs for their ability to inhibit the function of this virus.[1,2] Tetracycline has been proposed as a strong candidate against SARS-CoV-2[3] due to its lipophilic nature, anti-inflammatory response, as well as its ability to chelate zinc species on matrix metalloproteinases. Tetracycline class antibiotics have also been shown to be effective in reducing the duration of ventilatory support and intensive care unit stay from acute respiratory distress syndrome,[4] while doxycycline has been suggested to be an important component in combination therapy for its antiviral properties.[5] Tetracycline as well as a broad band of related antibiotics have been approved by the FDA.[6]

In this study, we quantify the performance of tetracycline in inhibiting the binding of the SARS-CoV-2 spike protein to the human receptor ACE2. This is of interest as SARS-CoV-2 initiates cell infection when the receptor-binding domain (RBD) of the viral spike

glycoprotein binds to the human cell receptor ACE2. The RBD of the S1 viral subunit comprises a two-stranded β5, β6 sheet that interacts strongly with ACE2 through persistent hydrogen bonding, leading to the remodeling of the S2 subunit from prefusion to postfusion state in preparation for membrane fusion.

In this study, we show that tetracycline can render the RBD–ACE2 complex an unstable, high energy configuration, such that the binding cascade triggering viral cell entry may be precluded.

Tetracycline is found to bind more favorably to the RBD compared to doxycycline, gentamicin, or chloroquine, which were included in this study as a baseline. The tetracycline–RBD complex also displays the lowest binding efficiency to the human cell receptor ACE2. As the RBD mediates the cell attachment and membrane fusion of the coronavirus to host cells, the blockage of RBD–ACE2 binding by tetracycline not only frames it as a strong therapeutic candidate but also as a template to understanding the crucial epitope features that can be leveraged to address the RBD with antibodies and vaccines.

2 | RESULTS AND DISCUSSION

2.1 | Binding character of the inhibitor–RBD complex

Tetracycline exhibits a higher binding affinity to the RBD in both blind and site-specific docking (−9.40 kcal/mol) compared to doxycycline (−8.08 kcal/mol), chloroquine (−6.63 vs. −6.31 kcal/mol), and gentamicin (−4.83 kcal/mol) as delineated in Table 1. The small molecule inhibitors examined bind stably to the RBD contact interface, as shown by the root mean square deviation (RMSD) and root mean square fluctuation (RMSF) profiles in Figure 1. Additionally, the RBD:ACE2 complex mediated by tetracycline appears to be the least dynamically stable compared to the uninhibited case as well as the protein–receptor complex in the presence of other inhibitors.

TABLE 1 The binding free energy of small-molecule inhibitors to the SARS-CoV-2 receptor-binding domain (RBD)

Inhibitor to RBD	ΔG_{bind} (kcal/mol)
Tetracycline	−9.40
Doxycycline	−8.08
Chloroquine	−6.31
Gentamicin	−4.83

Note: Tetracycline binds preferably to the RBD

The amino acid residues of the RBD involved in hydrogen bonding with the tetracycline molecule are Tyr 449, Asn 501, Gly 496, and Tyr 505 (Figure 2), which have been shown to be major hotspots involved in binding between the SARS-CoV- 2 RBD and ACE2 receptor.[7,8] These four residues are each part of the 17 total residues on the contact surface of the RBD that form persistent hydrogen bonds with ACE2.

Tyrosine residues are known to play an important role in mediating molecular contact and recognition at protein interfaces.[9] Likely due to its versatile, amphipathic interactions and low side-chain entropy, tyrosine is the most commonly occurring residue at the contact surface of the SARS-CoV-2 RBD. Tetracycline has been shown in experiments to bind favorably to tyrosine,[10,11] and we have demonstrated that it preferentially occupies half of the tyrosine residues at the RBD contact interface via both blind and targeted docking.

In the absence of inhibitors, the RBD residue Tyr 449 engages in hydrogen bonding with its polar hydroxyl group to Asp 38 and Gln 42 of ACE2, while the RBD residue Tyr 505 does the same with Lys 353, Arg 393, and Glu 37 of ACE2. The contact profiles of each tyrosine residue on the RBD account for a significant percentage of the buried surface area (14.8% and 18.0%, respectively, of the total buried surface area spanning nearly 18 nm^2 between ACE2 and RBD). The prominent role of such tyrosine residues in binding to ACE2 is a shared feature with the SARS-CoV RBD.[8] By binding to Tyr 449 and Tyr 505 on the RBD contact surface, tetracycline abolishes both the molecular specificity and affinity offered by these tyrosine residues in modulating the RBD–ACE2 complex.[9]

The RBD residue Asn 501 hydrogen bonds to Tyr 41 and Lys 353 of ACE2, occupying a buried surface area of 10.1%, while the RBD residue Gly 496 residue bonds with Lys 353 on ACE2 as well, with a buried surface area of 7.8%. The occupation of these two RBD residues by tetracycline is consistent with experimental, intracellular observations that asparagine and glycine residues bind favorably to tetracycline.[11] From a function standpoint, the small amino acid glycine is known to complement tyrosine in controlling molecular recognition.[9] Thus by blocking the Gly 496 and Asn 501 polar contact residues on the RBD,[12] tetracycline strongly inhibits formation of the RBD–ACE2 complex, a necessary precursor to cell and viral membrane fusion.

In comparison, the amino acids of RBD that interact with chloroquine in the site-specific configuration are Lys 356, Arg 454, Arg 466, and Arg 355, of which none are involved in extended hydrogen bonding with ACE2. For gentamicin, a hydrophilic aminoglycoside, the RBD residues that contribute the most to the binding energy with gentamicin are Lys 417, Glu 484, Lys 444, and Tyr 505. By occupying three contact RBD residues that

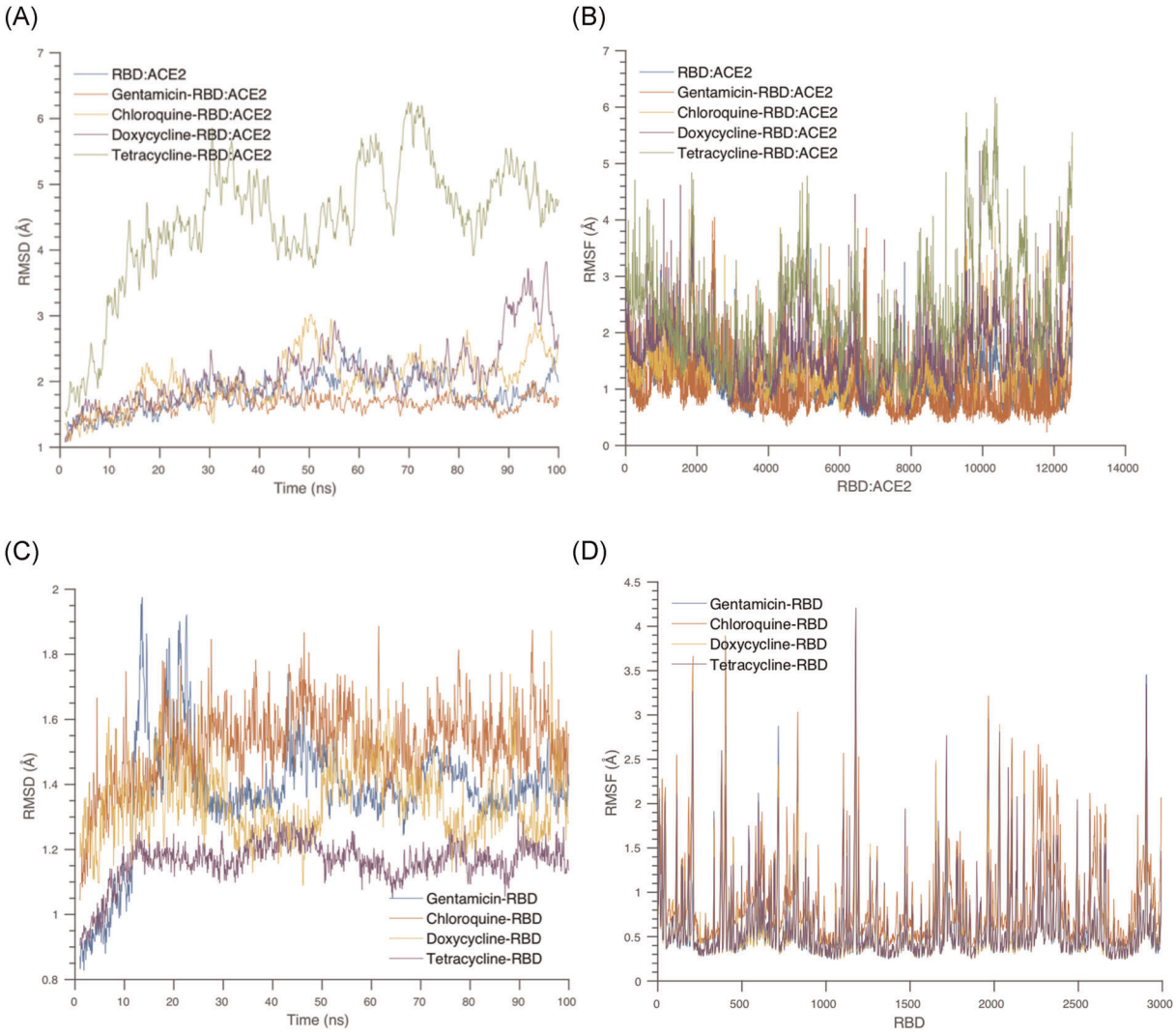

FIGURE 1 (A) RMSD plots of the RBD–ACE2 complex with and without the presence of small molecule inhibitors. The dynamic stability of the tetracycline–RBD:ACE2 structure appears distinctly lower than the uninhibited case, suggesting that the bound state is highly unfavorable. (B) RMSF of the RBD:ACE2 complex with and without inhibitors. (C) RMSD graphs of the inhibitor–RBD complex. Initial structures after equilibration are confirmed to be stable. (D) RMSF of the RBD when bound to small molecule inhibitors. Each structure is again shown to be stable over the trajectories run. ACE2, angiotensin-converting enzyme 2; RBD, receptor-binding domain; RMSD, root mean square deviation; RMSF, root mean square fluctuation

engage in hydrogen bonding with the human receptor ACE2 (Lys 417, Glu 484, Tyr 505), gentamicin can be expected to inhibit the RBD–ACE2 complex with greater efficacy than chloroquine. However, the affinity of gentamicin to the viral RBD is the lowest among the small molecules examined due to its high energy interaction with the RBD residues Ser 494 and Arg 403, two central amino acids in the binding pocket. This causes gentamicin to be displaced easily from the binding site and makes it a poor inhibitor of the RBD–ACE2 complex on average. Thus, tetracycline occupies the best position along the Pareto frontier in binding most favorably to the viral RBD, while also inhibiting formation of the RBD–ACE2 to the most significant degree.

Tetracycline binds preferably to polar or slightly lipophilic RBD residues, which as observed in the experiment comprise the majority of amino acids that form persistent hydrogen bonds with ACE2.[7,8,12,12,13] Other tetracycline derivatives such as doxycycline or minocycline are known to be more lipophilic[3,6,13] and may therefore prefer nonpolar residues[14] that are often buried beneath the solvent accessible surface area of the spike protein. Indeed, the RBD residues that have the highest binding affinity to doxycycline are Tyr 449, Gly 447, Val 445, Gly 496, of which only two are RBD amino acids that engage in persistent hydrogen bonding with ACE2. These two RBD residues Tyr 449 and Gly 496 were characterized earlier due to their interaction with tetracycline.

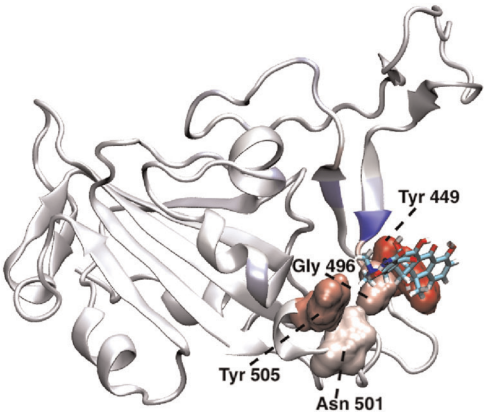

FIGURE 2 Interaction map of amino acid residues of the severe acute respiratory syndrome coronavirus 2 RBD that have the highest binding affinity with tetracycline. The Tyr 449, Asn 501, Gly 496, and Tyr 505 residues have also been shown to form persistent hydrogen bonds in maintaining the RBD–ACE2 complex.[7] ACE2, angiotensin-converting enzyme 2; RBD, receptor-binding domain

Lastly, the Lys 353 residue in human ACE2 is known to play a crucial role in SARS-CoV-2 recognition of the receptor[15]; the RBD residues that engage in extended hydrogen bonding with Lys 353 in human ACE2 may therefore be optimal targets for inhibition by drug and vaccine candidates to weaken the RBD–ACE2 complex. Indeed, tetracycline occupies two such RBD residues (Gly 496 and Asn 501), which may contribute to its strong inhibitory effect.

2.2 | Binding efficiency of the inhibited RBD–ACE2 complex

The binding efficiency[16] (magnitude of binding energy normalized by contact interface area) of the SARS-CoV-2 RBD–ACE2 complex was found to be 7.58 kcal/(mol nm^2). In the presence of the protein–ligand complex tetracycline–RBD, the binding efficiency with ACE2 (2.98 kcal/(mol nm^2)) is significantly lower than that for doxycycline–RBD (5.16 kcal/(mol nm^2)), chloroquine–RBD (5.59 kcal/(mol nm^2)) and gentamicin–RBD (7.02 kcal/(mol nm^2)) as displayed in Table 2. The statistical significance in the ranking of the mean binding efficiency to ACE2 for each RBD complex (from highest to lowest: RBD, gentamicin–RBD*, chloroquine–RBD**, doxycycline–RBD*, tetracycline–RBD**) was confirmed at the 5% (single asterisk) and 1% (double asterisk) level via a one-tailed, two-sample *t*-test between each inhibitor complex (e.g., tetracycline–RBD) and the complex with the nearest, higher binding efficiency (e.g., doxycycline–RBD).

TABLE 2 The binding efficiency[17] (magnitude of binding energy normalized by contact interface area) of the spike protein RBD as well as the tetracycline–RBD, doxycycline–RBD, gentamicin–RBD, and chloroquine–RBD complexes to the human cell receptor ACE2

Complex to ACE2	Binding efficiency (kcal/(mol nm^2))
RBD	7.58
Gentamicin–RBD	7.02 *
Chloroquine–RBD	5.59 **
Doxycycline–RBD	5.16 *
Tetracycline–RBD	2.98 **

Note: Binding efficiency is the lowest for the tetracycline–RBD complex, indicating that tetracycline is a more effective inhibitor. The statistical significance in the ranking of mean binding efficiency to ACE2 for each RBD complex was confirmed at the *5% and **1% level via a one-tailed, two-sample *t*-test between each inhibitor complex (e.g., tetracycline–RBD) and the complex with the nearest, higher binding efficiency (e.g., doxycycline–RBD).

The relationship between optimal binding efficiency between a protein and ligand to the buried surface area was explored by Day et al.,[8] who found that approximately 5 nm^2 was the minimum contact area necessary to sustain a stable receptor ligand complex. This area threshold arises from a survey of 152 protein–protein complexes and is theorized to generate sufficient binding energy to offset the loss in configurational entropy of the individual unbound proteins. In this vein, we find that the buried surface area for the inhibited ligand gentamicin-RBD to the human receptor ACE2 is 7.52 nm^2, chloroquine–RBD to ACE2 is 6.53 nm^2, doxycycline–RBD to ACE2 is 4.78 nm^2, and tetracycline–RBD to ACE2 is 3.39 nm^2. This suggests that the doxycycline–RBD and tetracycline–RBD ligands do not support sufficient buried surface area with ACE2 to sustain a minimally stable complex on longer time scales.

The reduction in contact area can be correlated with the decrease of hydrogen bonding activity between the inhibited RBD and ACE2. A survey of hydrogen bonding lifetimes between the important binding site residues in the RBD with ACE2[7] shows that the tetracycline inhibited RBD exhibits the least hydrogen bonding activity with ACE2 (Figure 3). As shown prior, the occupation of polar contact residues of the RBD by tetracycline allows it to block the binding of the RBD to ACE2 to a greater degree.

2.3 | Dissociation PMF of the RBD–ACE2 complex

To verify the strong inhibition of the RBD–ACE2 complex by tetracycline, steered molecular dynamics

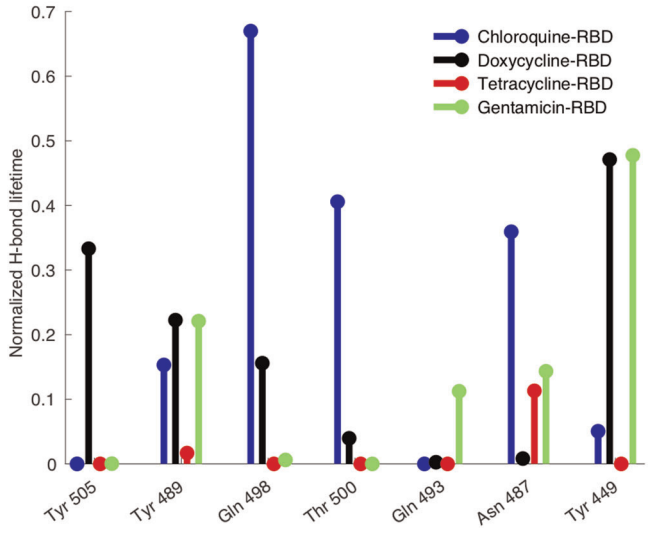

FIGURE 3 The hydrogen bonding lifetimes of binding site residues of the inhibited RBD with ACE2 sustained in 100 ns of simulation time, normalized by hydrogen bonding lifetimes in the uninhibited RBD–ACE2 complex. ACE2, angiotensin-converting enzyme 2; RBD, receptor-binding domain

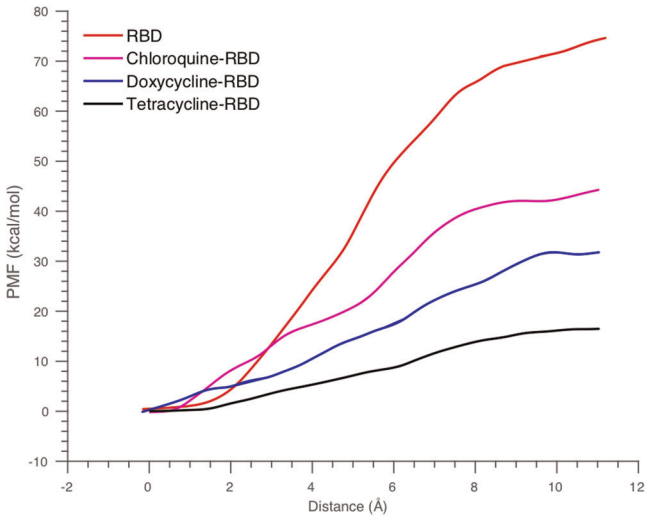

FIGURE 4 The PMF as a function of the distance between the centers of masses of the spike protein RBD complexes and the cell receptor ACE2. The tetracycline–RBD complex exhibits the lowest free energy profile along the dissociation pathway.
ACE2, angiotensin-converting enzyme 2; PMF, potential of mean force; RBD, receptor-binding domain

simulations were carried out to find the potential of mean force (PMF) along a single dissociation pathway for the inhibited and uninhibited RBD-ACE2 complexes. The PMF approximates the diffusive free energy profile along the direction normal to the effective contact plane of the inhibited viral RBD and receptor ACE2.

Figure 4 shows that the PMF for unbinding of the tetracycline–RBD complex from ACE2 was the lowest of the four structures tested, which is in agreement with the binding efficiencies found from equilibrium simulations. From the reaction path of the inhibited RBD, the dominant contribution to the energy barrier of dissociation is found to be localized at the N-terminal small lobe of ACE2, which interacts with residue Tyr 484 and Asn 487 on the RBD. Given the strong polar affinity of the tetracycline molecule and its demonstrated binding preference for tyrosine and asparagine, this secondary site may be another target for inhibition, though a full analysis is out of the scope of this study. The blockage of polar residues at the RBD–ACE2 interface by tetracyclines may therefore preclude cell entry initiated during binding of the viral spike protein to ACE2.

3 | METHODS

3.1 | Docking

The SARS-CoV-2 RBD, ACE2, tetracycline, and chloroquine molecular structures were obtained from RCSB PDB (6M0J, 2UXO, 4V2O, 2XRL).[8,16,19,20] Missing hydrogen atoms were appended, after which structural preparation (cleaning and relaxation) and molecular docking with full ligand and protein backbone flexibility were carried out using the Rosetta 3.7.[17,21,22] The ensemble of 100 ligand conformers were sampled using the BioChemical Library (BCL 3.2)[23] which draws on a library of rotamers for common fragments in organic molecules. This scheme gives locally equilibrated geometries with nonlocal interactions governed by a clash score that penalizes atomic overlap. The parameter files containing partial charges, bond lengths, atom types, and torsion angles were populated with the Rosetta script molfile_to_params.py.

The three output files—a pdb of the original molecule, a parameter file, and the conformer library—were used to perform protein–ligand docking with RosettaLigand.[17,21] This procedure starts with low resolution, rigid body docking comprising 500 cycles of translation and rotation followed by distance minimization of the ligand to the protein to satisfy a Lennard-Jones interaction and atomic clash score.[17] Then the structure is subjected to six cycles of high-resolution docking that samples the ensemble of side-chain rotamers singly and simultaneously for multiple side chains.[17] This repacking is coupled with incremental shifts of the ligand position and orientation, after which the structures and torsion angles of the ligand and protein side chains are minimized with respect to a "soft" repulsive scoring function at the end of each cycle.[21] Finally, the protein/ligand

complex, including flexible residue backbones on the protein receptor, was minimized with respect to a "hard" repulsive scoring function that discards conformers with large clash elements.

One thousand output models were produced for each ligand–protein complex. Each model is assessed with a total score function that takes into account the hydrogen bonding potential, electrostatics, van der Waals forces, and implicit solvent interactions. The three lowest scoring models for each complex were used as initial conditions for a second docking pass, producing 150 second generation models for each initial condition. An interface score is then calculated as the difference in hard repulsion energy between the ligand–protein complex and the separated species where the ligand is shifted away from the protein. From the 10 second generation models with the lowest total scores, the complex with the lowest interface score was chosen for further analysis.

3.2 | Binding free energy

The binding affinities of the best-scoring models for each ligand–protein complex were gauged using MM/PBSA calculations after 100 ns equilibrium molecular dynamics simulations.[24–26] First, each complex was parameterized using CHARMM36 with CMAP cross terms.[27] Then, the ligand–protein structure was solvated in 83,000 TIP3P water and neutralized with sodium and chloride ions in a fully periodic box with dimensions $12 \times 12 \times 22\,\mathrm{nm}^3$. Relaxation runs over 10 ns were completed in the NVT ensemble, before production runs for binding energy computations. Here, the temperature was controlled via the velocity rescaling algorithm over a relaxation timescale of 1 ps. Over the course of the relaxation runs, the backbone of the protein as well as the ligand were tethered to their initial position with an energetic penalty of 100 kJ/mol. The simulation time step was set to 2 fs.

Finally, equilibrium simulations were performed at 300K and 1 bar using the Nosé-Hoover thermostat with relaxation timescale 1 ps and Parrinello-Rahman barostat with a relaxation timescale of 2 ps. Long-distance electrostatics were accounted for with the Particle Mesh Ewald algorithm across periodic boundary conditions in all three dimensions. The simulation timestep was likewise held to 2 fs.

In brief, the binding free energy of the ligand to the protein can be found via[25]

$$\Delta G_{\mathbf{binding}} = G_{\mathbf{complex}} - G_{\mathbf{protein}} + G_{\mathbf{ligand}}, \quad (1)$$

where the right-hand side expresses the free energy of the protein–ligand complex in solvent, the protein in solvent, and the ligand in solvent, respectively. The total energy of each species can be found from

$$\Delta G_{\mathbf{sp}} = \langle E_{\mathbf{MM}} \rangle - TS + \langle G_{\mathbf{solvation}} \rangle. \quad (2)$$

Here, the subscript sp is the complex, protein or ligand. The term $\langle E_{\mathbf{MM}} \rangle$ is the ensemble average of the vacuum molecular mechanics energy, *TS* gives the conformational entropy, and $\langle G_{\mathbf{solvation}} \rangle$ is the solvation free energy. The entropic contribution *TS* is typically neglected due to the significant computational cost.[25,26]

The potential energy $E_{\mathbf{MM}}$ can be expressed as the sum of the force field parameters

$$E_{\mathbf{MM}} = E_{\mathbf{bonded}} + E_{\mathbf{vdW}} + E_{\mathbf{elec}}, \quad (3)$$

where the right-hand side contains the bonded interactions (bond, angle, dihedral and improper energies), van der Waals interactions, and electrostatic interactions. The solvation energy $G_{\mathbf{solvation}}$ can be decomposed into polar and nonpolar terms

$$G_{\mathbf{solvation}} = G_{\mathbf{polar}} + G_{\mathbf{nonpolar}}. \quad (4)$$

The polar component of the solvation energy can be found by solving the Poisson–Boltzmann equation, while the nonpolar component is typically modeled as

$$G_{\mathbf{nonpolar}} = G_{\mathbf{cavity}} + G_{\mathbf{vdW}}. \quad (5)$$

The first term represents the work done to form a cavity in the surrounding solvent, while the second gives the attractive component of the van der Waals interactions between the solute and solvent. These calculations are performed in GROMACS[24–26] to give the binding free energy between the ligand and protein.

3.3 | RBD:ACE2 complex

After the inhibitor–RBD system is relaxed, flexible protein–protein docking is performed using Rosetta docking protocols[28] to gauge the conformational stability of the inhibitor–RBD–ACE2 complex. The ACE2 receptor was first repacked to remove clashes, and the best scoring conformation out of 10 models was selected for subsequent docking. The uninhibited RBD–ACE2 complex served as a template for the initial orientation of the ACE2 receptor with the inhibitor–RBD structure, except that the ACE2 protein is displaced normal to the binding interface to minimize clashing with the inhibitor.

Finally, the inhibitor–RBD structure was docked to the ACE2 via a coarse resolution search stage that rotates and translates the centroids of the two proteins, followed by a high resolution, full atom search that samples a rotamer library of protein side chains. Lastly, the binding interface was minimized with respect to the Talaris score

function to generate output 500 models. The best score model was used in subsequent calculations for the binding efficiency.

The inhibitor–RBD–ACE2 complex was then examined using equilibrium molecular dynamic simulations in GROMACS with the procedure described earlier. After sampling 100 ns of the isothermal-isobaric ensemble, the binding free energy was found from the MMPBSA method and normalized with respect to the area of the buried surface area at the interface. This gave the binding efficiency of the complex.

3.4 | The potential of mean force

The PMF[29] along the dissociation pathway of the inhibitor–RBD structures from ACE2 were found in LAMMPS[30] using steered molecular dynamics. The reaction coordinate was chosen to be the difference between the center of mass (COM) of the RBD main-chain backbone from the COM of the ACE2 backbone projected onto the axis normal to the plane of their binding interface. A pulling speed of 10 Å/ns and spring constant of 1300 pN/Å was used to abide by the stiff spring approximation while avoiding irreversible distortions of the ligand during dissociation. The canonical ensemble was sampled by holding the temperature fixed at 300K using a Nosé-Hoover thermostat with a relaxation timescale of 1 ps. The system was solvated with 83,500 TIP3P water molecules across periodic boundary conditions in all orthogonal directions. As before, long-distance electrostatics were accounted for with the Particle Mesh Ewald algorithm. Finally, Jarzynski's equality was employed to calculate the free energy profile for each inhibitor–RBD structure from 10 trajectories statistically independent initial conditions, sampled at 20 ns intervals from an equilibrium canonical ensemble.[31]

4 | CONCLUSIONS

The tetracycline class of antibiotics, including tetracycline, oxytetracycline, and doxycycline may be helpful in the fight against the coronavirus SARS-CoV-2, due to its preferential association with the important residues in the viral receptor-binding domain and the resulting strong inhibition of the RBD–ACE2 complex. Further experimental studies are recommended to validate how this reduction of cellular infection complements or enhances the anti-inflammatory and antiviral properties of tetracyclines in their role as a treatment for SARS-CoV-2.

CONFLICT OF INTERESTS

The authors declare that there are no conflict of interests.

AUTHOR CONTRIBUTIONS

Tom Y. Zhao conceived and planned the research, as well as performed calculations. Neelesh A. Patankar and Tom Y. Zhao performed analysis and wrote the manuscript.

DATA AVAILABILITY STATEMENT

The data that support the findings of this study are available from the corresponding author upon reasonable request.

ORCID

Tom Y. Zhao https://orcid.org/0000-0002-7708-0585

REFERENCES

1. Muhammad A, Ghazanfar A. Docking study of chloroquine and hydroxychloroquine interaction with rna binding domain of nucleocapsid phospho-protein—an in silico insight into the comparative efficacy of repurposing antiviral drugs. *J Biomol Struct Dyn*. 2020:1-13. https://doi.org/10.1080/07391102.2020.1775703
2. Sekiou O, Bouziane I, Bouslama Z, Djemel A. In-silico identification of potent inhibitors of COVID-19 main protease (Mpro) and angiotensin converting enzyme 2 (ACE2) from natural products: quercetin, hispidulin, and cirsimaritin exhibited better potential inhibition than hydroxy-chloroquine against COVID-19 main protease active site and ACE2. 2020. https://doi.org/10.26434/chemrxiv.12181404
3. Sodhi M, Etminan M. Therapeutic potential for tetracyclines in the treatment of covid-19. *Pharmacotherapy: J Human Pharmacol Drug Therapy*. 2020;40(5):487-488.
4. Byrne JD, Shakur R, Collins J, et al. Prophylaxis with tetracyclines in ards: potential therapy for covid-19-induced ards? *medRxiv*. 2020. https://doi.org/10.1101/2020.07.22.20154542
5. Malek AE, Granwehr BP, Kontoyiannis DP. Doxycycline as a potential partner of covid-19 therapies. *IDCases*. 2020;21:e00864.
6. Yates PA, Leone AM, Reichel E. A proposed randomized, double blind, placebo controlled study evaluating doxycycline for the prevention of covid-19 infection and disease in healthcare workers with ongoing high risk exposure to covid-19. *medRxiv*. 2020. https://doi.org/10.1101/2020.05.11.20098525
7. Veeramachaneni GK, Thunuguntla VBSC, Bobbillapati J, Bondili JS. Structural and simulation analysis of hotspot residues interactions of sars-cov 2 with human ace2 receptor. *J Biomol Struct Dyn*. 2020:1-11. https://doi.org/10.1080/07391102.2020.1773318
8. Lan J, Ge J, Yu J, et al. Structure of the sars-cov-2 spike receptor-binding domain bound to the ace2 receptor. *Nature*. 2020;581(7807):215-220.
9. Koide S, Sidhu SS. The importance of being tyrosine: lessons in molecular recognition from minimalist synthetic binding proteins. *ACS Chem Biol*. 4(5):325-334. https://doi.org/10.1021/cb800314v
10. Xu Q, Han B, Wang H, Wang Q, Zhang W, Wang D. Effect of extracellular polymer substances on the tetracycline removal

during coagulation process. *Bioresour Technol*. 2020;309: 123316.
11. Freeman BA, Circo R. Effect of tetracyclines on the intracellular amino acids of molds. *J Bacteriol*. 1963;86(1): 38-44. https://doi.org/10.1128/JB.86.1.38-44.1963
12. Wang Q, Zhang Y, Wu L, et al. Structural and functional basis of sars-cov-2 entry by using human Ace2. *Cell*. 2020;181(4):894–904.
13. Du Q-S, Li D-P, He W-Z, Chou K-C. Heuristic molecular lipophilicity potential (hmlp): lipophilicity and hydrophilicity of amino acid side chains. *J Comput Chem*. 2006;27(6):685-692.
14. Gautieri A, Beeg M, Gobbi M, Rigoldi F, Colombo L, Salmona M. The anti-amyloidogenic action of doxycycline: a molecular dynamics study on the interaction with aB42. *Int J Mol Sci*. 2019;20(18):4641.
15. Wan Y, Shang J, Graham R, Baric RS, Li F, Gallagher T. Receptor recognition by the novel coronavirus from wuhan: an analysis based on decade-long structural studies of sars coronavirus. *J Virol*. 2020;94(7):e00127.
16. Huta BP, Mehlenbacher MR, Nie Y, et al. The lysosomal protein saposin b binds chloroquine. *ChemMedChem*. 2016; 11(3):277-282.
17. Davis IW, Baker D. Rosettaligand docking with full ligand and receptor flexibility. *J Mol Biol*. 2009;385(2):381-392.
18. Day ES, Cote SM, Whitty A. Binding efficiency of protein-protein complexes. *Biochemistry*. 2012;51(45):9124-9136.
19. Palm GJ, Buchholz I, Werten S, et al. Thermodynamics, cooperativity and stability of the tetracycline repressor (tetr) upon tetracycline binding. *Biochim Biophys Acta (BBA)*. 2020; 1868(6):140404.
20. Alguel Y, Meng C, Terán W, et al. Crystal structures of multidrug binding protein ttgr in complex with antibiotics and plant antimicrobials. *J Mol Biol*. 2007;369(3):829-840.
21. Lemmon G, Meiler J. Rosetta ligand docking with flexible xml protocols. *Methods Mol Biol*. 2012;819:143-155.
22. Meiler J, Baker D. Rosettaligand: protein-small molecule docking with full side-chain flexibility. *Proteins*. 2006;65(3):538-548.
23. Kothiwale S, Mendenhall JL, Meiler J. Bcl::conf: small molecule conformational sampling using a knowledge based rotamer library. *J Cheminf*. 2015;7:47.
24. Berendsen HJC, van der Spoel D, van Drunen R. Gromacs: a message-passing parallel molecular dynamics implementation. *Comput Phys Commun*. 1995;91(1):43-56.
25. Kumari R, Kumar R, Lynn A. g_mmpbsa—a gromacs tool for high-throughput mm-pbsa calculations. *J Chem Inf Model*. 2014;54(7):1951-1962.
26. Lindahl E, Hess B, Spoel D. Gromacs 3.0: a package for molecular simulation and trajectory analysis. *Molecular Model Annual*. 2001;7(8):306-317.
27. Brooks BR, Brooks CL 3rd, Mackerell AD Jr, et al. Charmm: the biomolecular simulation program. *J Comput Chem*. 2009; 30:1545-1614.
28. Lewis SM, Kuhlman BA. Anchored design of protein-protein interfaces. *PLOS One*. 2011;6(6):e20872. https://doi.org/10.1371/journal.pone.0020872
29. Chen P-C, Kuyucak S. Accurate determination of the binding free energy for kcsacharybdotoxin complex from the potential of mean force calculations with restraints. *Biophys J*. 2011; 100(10):2466-2474.
30. Plimpton S. Fast parallel algorithms for short-range molecular dynamics. *J Comput Phys*. 1995;117(1):1-19.
31. Dellago C, Hummer G. Computing equilibrium free energies using non-equilibrium molecular dynamics. *Entropy*. 2013; 16(41–61):12-61.

How to cite this article: Zhao TY, Patankar NA. Tetracycline as an inhibitor to the SARS-CoV-2. *J Cell Biochem*. 2021;122:752–759. https://doi.org/10.1002/jcb.29909